

Antiaromaticity versus Electron Affinity: Quantitative Insights into Metal–Ligand Interactions in Ni–Pentalene Complexes

Riina Kuwata,^{a,‡} Takefumi Imanishi,^{a,‡} Shota Hasegawa,^b Zhe Wang,^b Junichi Usuba,^b Kosuke Yasui,^b Yuta Uetake,^{c,d*} and Aiko Fukazawa^{b*}

^a Department of Energy and Hydrocarbon Chemistry, Graduate School of Engineering, Kyoto University, Yoshida, Sakyo-ku, Kyoto 606-8501, Japan

^b Institute for Integrated Cell-Material Sciences (WPI-iCeMS), Institute for Advanced Study, Kyoto University, Yoshida, Sakyo-ku, Kyoto 606-8501, Japan

^c Department of Applied Chemistry, Graduate School of Engineering, The University of Osaka, Suita, Osaka 565-0871, Japan

^d Innovative Catalysis Science Division, Institute for Open and Transdisciplinary Research Initiatives (ICS-OTRI), The University of Osaka, Suita, Osaka 565-0871, Japan

‡ R.K. and T.I. contributed equally to this work.

ABSTRACT: Transition metal complexation has long served as a strategy for stabilizing antiaromatic hydrocarbons. However, the underlying factors that govern their coordination behavior are not yet fully understood. In this study, we synthesized and characterized a Ni(0) complex, [Ni(cod)(1)], featuring a benzothiophene-*S,S*-dioxide-fused pentalene ligand, and compared it to a structurally analogous complex, [Ni(cod)(2)], bearing a more antiaromatic but less electron-accepting pentalene. Through a combination of experimental and computational approaches, including single-crystal X-ray diffraction, X-ray absorption spectroscopy, variable-temperature NMR, and energy decomposition analysis, we found that the enhanced stability of [Ni(cod)(1)] is primarily associated with substantial π -back donation facilitated by its low-lying LUMO, rather than by the relief of antiaromatic destabilization. Notably, [Ni(cod)(1)] also exhibits pronounced fluxional behavior in solution, involving reversible migration of the Ni center between the two fused five-membered rings. DFT calculations suggest that this dynamic process is coupled with the shifting of C=C bonds within the pentalene framework. These findings illustrate that focusing on quantifiable electronic features provides a more nuanced and predictive understanding of antiaromatic coordination chemistry, while also revealing dynamic behaviors that may be intrinsic to antiaromatic frameworks.

INTRODUCTION

Transition metal complexes with antiaromatic hydrocarbons as ligands have long been studied as a method for the stabilization and isolation of otherwise unstable antiaromatic hydrocarbons. For instance,

while pristine cyclobutadiene and pentalene are extremely labile even under cryogenic temperatures,^{1,2} numerous corresponding transition metal complexes have been successfully synthesized and characterized (Figure 1a,b).^{3–10} The driving force behind the coordination of these antiaromatic hydrocarbons to transition metals has long been qualitatively attributed to the relief of antiaromatic destabilization or the acquisition of aromatic stabilization.⁷ On the other hand, the coordination bonds between transition metals and olefin ligands, including cyclic 4nπ electron systems, have long been recognized to involve π-back donation playing a crucial role.^{5b,11} Given the exceptionally low LUMO energy levels of antiaromatic hydrocarbons compared to other unsaturated hydrocarbons, it is reasonable to hypothesize that such distinctive electronic structures contribute to their strong interactions with transition metals. Surprisingly, however, it remains unclear which factor plays a more significant role in the thermodynamic stabilization of antiaromatic hydrocarbons upon metal coordination: the relief of antiaromatic destabilization or the strong π-back donation enabled by the exceptionally low-lying LUMOs. Distinguishing between these contributions would help advance understanding of the fundamental nature of antiaromatic hydrocarbons as ligands.

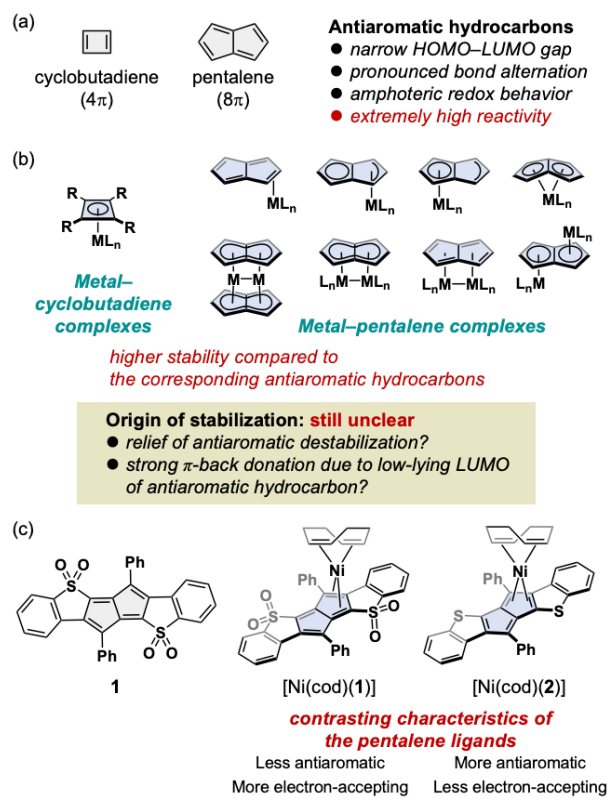
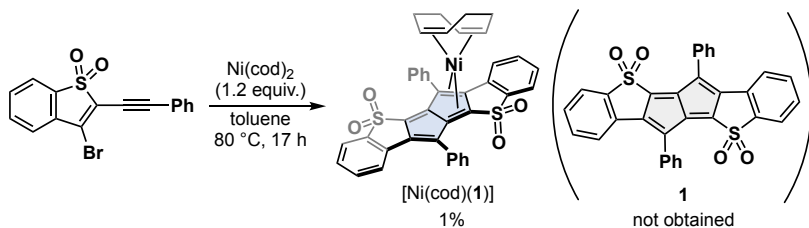


Figure 1. (a) Representative antiaromatic hydrocarbons: cyclobutadiene and pentalene, and their characteristic features. (b) Transition metal complexes bearing antiaromatic hydrocarbons as ligands, shown with generalized structural formulas that highlight coordination mode variations rather than specific metal centers. (c) Molecular structures of benzothiophene-S,S-dioxide-fused pentalene **1** and the two relevant Ni complexes [Ni(cod)(1)] and [Ni(cod)(2)] investigated in this study.

As a clue to addressing this fundamental question, we serendipitously obtained a Ni complex bearing a benzothiophene-*S,S*-dioxide-fused pentalene (**1**) as a ligand, i.e., [Ni(cod)(**1**)] (cod: 1,5-cyclooctadiene), while conducting research for a different purpose (Figure 1c). We herein report the synthesis and characterization of [Ni(cod)(**1**)] and its analogous complex [Ni(cod)(**2**)], along with the quantitative investigations of the metal–ligand interactions. These complexes enabled a quantitative comparison to identify whether the degree of antiaromatic character or the energy levels of the frontier molecular orbitals of the ligands predominantly govern the strength of the coordination bonds between pentalene moieties and Ni. Furthermore, we also examined the fluxional behavior of Ni–pentalene complex [Ni(cod)(**1**)].

RESULTS AND DISCUSSION

Serendipitous Formation and Structural Characterization of [Ni(cod)(1**)].** The Ni complex [Ni(cod)(**1**)] was unexpectedly obtained during the attempted synthesis of a benzothiophene-*S,S*-dioxide-fused pentalene **1** (Scheme 1). Based on the reaction conditions for the synthesis of dithieno[*a,e*]pentalene derivatives,^{12,13} we performed dimerization of 3-bromo-2-(phenylethynyl)benzothiophene-*S,S*-dioxide using a stoichiometric amount of Ni(cod)₂. As a result, while the desired pentalene **1** was not obtained, the corresponding Ni complex [Ni(cod)(**1**)] was isolated in a low yield of 1% as dark green crystals from a complex reaction mixture. Single-crystal X-ray diffraction studies of [Ni(cod)(**1**)] revealed that both cyclooctadiene and **1** adopt η^4 -coordination to the Ni center (Figure 2a, *vide infra*). Based on the conventional ionic model, a tetrahedral geometry of the Ni center, as well as the well-defined NMR resonance signals in ¹H NMR (Figure S17 in Supporting Information), the formal oxidation number of the Ni center is characterized to be zero.¹⁴ Remarkably, [Ni(cod)(**1**)] exhibited reasonable stability under ambient conditions and was resistant to the purification process using a standard silica gel column chromatography technique in the air. This stability is in sharp contrast to the air-sensitive nature of conventional Ni(0)–olefin complexes, such as Ni(cod)₂. The observed stability of [Ni(cod)(**1**)] is reminiscent of the air-stable Ni(0) complexes recently reported, such as [Ni(^Rstb)₃]¹⁵ and [Ni(cod)(dq)]¹⁶ (^Rstb: substituted stilbene; dq: duroquinone), bearing electron-accepting olefinic ligands (Figure 2c).



Scheme 1. Serendipitous synthesis of [Ni(cod)(**1**)].

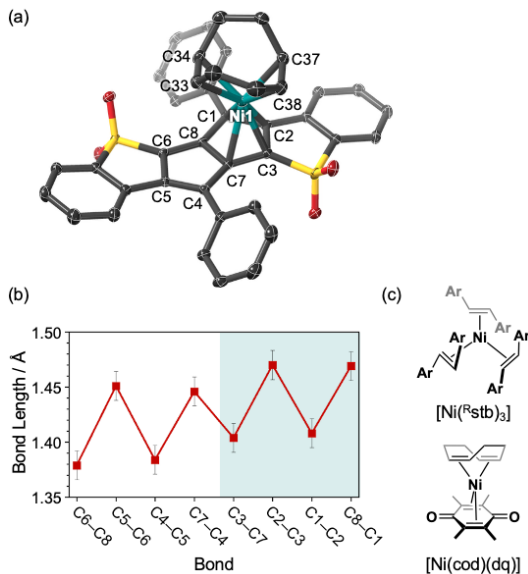


Figure 2. (a) Molecular structure of $[\text{Ni}(\text{cod})(\mathbf{1})]$ determined by single-crystal X-ray diffraction analysis (thermal ellipsoids drawn at 50% probability; black, carbon; red, oxygen; yellow, sulfur; green, nickel). Hydrogen atoms and solvent molecules are omitted for clarity. (b) Plot of selected C–C bond lengths in the crystal structure of $[\text{Ni}(\text{cod})(\mathbf{1})]$. Error bars represent standard deviations. The five-membered ring proximal to Ni is highlighted in green. (c) Representative examples of recently reported air-stable Ni(0)–olefin complexes $[\text{Ni}({}^{\text{R}}\text{stb})_3]$ and $[\text{Ni}(\text{cod})(\text{dq})]$ (${}^{\text{R}}\text{stb}$ = substituted stilbene; dq = duroquinone).

Detailed analysis of the crystal structure of $[\text{Ni}(\text{cod})(\mathbf{1})]$ revealed key features of its coordination geometry (Figure 2a,b, and Table S1). The pentalene framework exhibits pronounced bond length alternation: the C–C bonds fused to the benzothiophene rings C2–C3 and C5–C6, and those at C8–C1 and C7–C4 are significantly longer (C2–C3: 1.470(3) Å; C5–C6: 1.451(3) Å; C8–C1: 1.468(3) Å; C7–C4: 1.446(3) Å), whereas the remaining C–C bonds are shorter (C1–C2: 1.408(3) Å; C3–C7: 1.404(3) Å; C4–C5: 1.384(3) Å; C6–C8: 1.379(3) Å). This pattern aligns with DFT calculations on the free ligand **1**, which predict greater stability for the isomer with longer C–C bonds at the fusion sites (Figure S6). In the five-membered ring near the Ni center (C1, C2, C3, C7, C8), the C–C bonds are generally longer than those in the opposite ring (C4, C5, C6, C8, C7), suggesting electronic perturbation due to coordination with the Ni atom. The Ni–C distances (Ni–C2: 2.124(2) Å, Ni–C3: 2.042(2) Å; Ni–C1: 2.242(2) Å, Ni–C7: 2.203(3) Å) are consistent with interaction between Ni and an *s-cis*-butadiene-type fragment (C1, C2, C3, C7). The geometry of this *s-cis*-butadiene-type fragment relative to the cyclooctadiene ligand indicates that the Ni center adopts a tetrahedral geometry, characteristic of Ni(0) complexes.

Design and Synthesis of $[\text{Ni}(\text{cod})(\mathbf{2})]$ Bearing a More Antiaromatic, Less Electron-Accepting Pentalene Ligand. To understand the origin of the unexpectedly high stability of $[\text{Ni}(\text{cod})(\mathbf{1})]$, we next

investigated whether this stability is more strongly influenced by the relief of antiaromatic character (or the gain in aromatic character) upon coordination, or substantial metal-to-ligand π -back donation driven by the high electron affinity of the ligand. To this end, we designed $[\text{Ni}(\text{cod})(\mathbf{2})]$, a structurally analogous Ni complex bearing benzothiophene-fused pentalene (**2**) as a ligand, as a suitable reference compound. Quantum chemical calculations revealed that **2** exhibits significantly stronger paratropicity than **1** ($\text{NICS}(1)_{zz} = +45.1 \text{ ppm}$ for **1**, $+61.8 \text{ ppm}$ for **2** at B3LYP/6-311+G(2d,p)//B3LYP/6-31G(d); Figures 3a and S10), while possessing a substantially higher LUMO energy level (-3.70 eV for **1**, -2.77 eV for **2** at B3LYP/6-31G(d); Figure 3b).¹⁷ Notably, although stronger antiaromatic character typically correlates with lower LUMO energy levels in many $4n\pi$ electron systems, the relationship between **1** and **2** represents a rare exception to this general trend (Figure S11 and Table S6), probably due to the strong electron-withdrawing effect of SO_2 moieties. Consequently, this pair of compounds is particularly valuable for clarifying the relative importance of the degree of antiaromatic character versus low-lying LUMO levels of the pentalene ligands for the stability of the corresponding Ni-pentalene complexes $[\text{Ni}(\text{cod})(\mathbf{1})]$ and $[\text{Ni}(\text{cod})(\mathbf{2})]$.

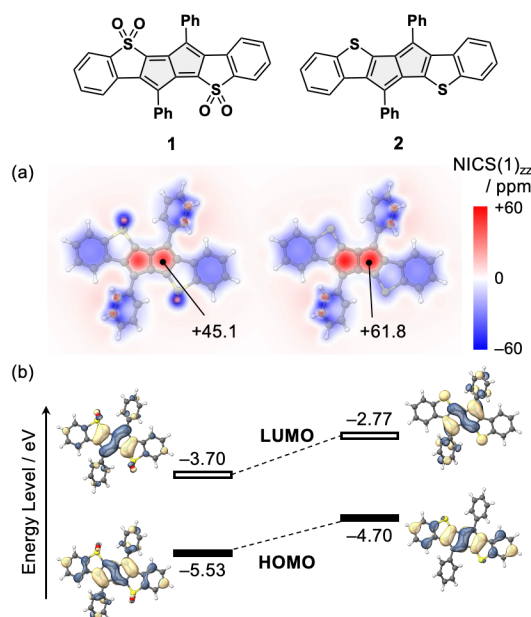


Figure 3. Comparison of the electron affinity and antiaromatic character between pentalene derivatives **1** and **2** based on the DFT calculations. The geometries used in all calculations were optimized at the B3LYP/6-31G(d) level of theory. (a) 2D $\text{NICS}(1)_{zz}$ map at 1 Å above XY plane, and $\text{NICS}(1)_{zz}$ values at the centroid of the five-membered ring, calculated at the B3LYP/6-311+G(2d,p)//B3LYP/6-31G(d) level of theory. (b) The Kohm-Sham HOMO and LUMO energy levels and their pictorial representations estimated at the B3LYP/6-31G(d) level of theory (isovalue = 0.03).

The complex $[\text{Ni}(\text{cod})(\mathbf{2})]$ was synthesized via a ligand exchange reaction between $\text{Ni}(\text{cod})_2$ and independently prepared **2** (Figure 4a). Monitoring of the reaction by ^1H NMR spectroscopy revealed that the signals corresponding to $\text{Ni}(\text{cod})_2$ disappeared over 8 hours at ambient temperature, while the signals assignable to dissociated 1,4-cyclooctadiene (COD) and a new species attributed to $[\text{Ni}(\text{cod})(\mathbf{2})]$ emerged without noticeable signals of side products (Figure 4b). The formation of $[\text{Ni}(\text{cod})(\mathbf{2})]$ was further supported by high-resolution mass spectrometry (Figure S22). In contrast, the NMR signals corresponding to $[\text{Ni}(\text{cod})(\mathbf{2})]$ rapidly disappeared upon exposure of the NMR sample to air (Figure 4c), indicating that this complex is significantly less stable than $[\text{Ni}(\text{cod})(\mathbf{1})]$ under ambient conditions. The calculated Gibbs free energy change (ΔG) for the ligand exchange reactions of $\text{Ni}(\text{cod})_2$ with either ligand **1** or **2** at the $\omega\text{B97X-D/def2-TZVP}$ level of theory was $-28.40 \text{ kcal mol}^{-1}$ for **1** and only $-12.01 \text{ kcal mol}^{-1}$ for **2** (Figure S7), supporting a greater thermodynamic stabilization for the formation of $[\text{Ni}(\text{cod})(\mathbf{1})]$. Collectively, these results suggest that the high stability of $[\text{Ni}(\text{cod})(\mathbf{1})]$ is more likely attributed to the low-lying LUMO of the ligand rather than the degree of antiaromatic character.

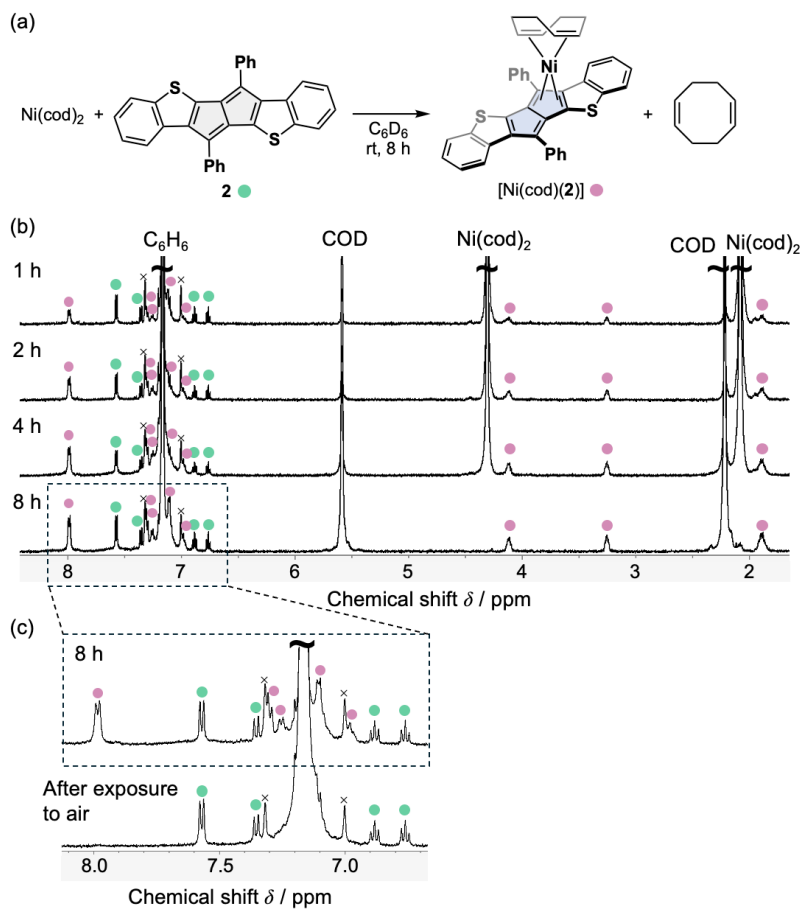


Figure 4. (a) Synthetic scheme of $[\text{Ni}(\text{cod})(\mathbf{2})]$ via ligand exchange reaction. (b,c) Time course of ^1H NMR spectra (500 MHz, in C_6D_6) of the reaction mixture recorded under an argon atmosphere (b), followed by spectral changes observed after exposure of the sample to air (c). Spinning side bands accompanied by the signal of C_6H_6 were marked with \times . COD: 1,4-cyclooctadiene.

Quantitative Analyses of π -Back Donation. To gain deeper insights into the strength of π -back donation from the Ni center to the pentalene ligands in these complexes, we conducted further experimental and theoretical investigations. Ni K-edge X-ray absorption spectroscopy (XAS) was performed for [Ni(cod)(1)], [Ni(cod)(2)], and [Ni(cod)(dq)] to evaluate the electronic state of the Ni centers. The overall feature of the X-ray absorption near edge structure (XANES) of [Ni(cod)(2)] closely resembles that of [Ni(cod)(1)] (Figure 5a), reflecting structural similarity in the vicinity of the Ni center. Although the structure of [Ni(cod)(2)] has not yet been fully characterized by single-crystal X-ray diffraction, its Ni center is expected to adopt an η^4 -coordination environment similar to that in [Ni(cod)(1)]. The pre-edge peak of [Ni(cod)(1)], which corresponds to the electric dipole-allowed Ni 1s \rightarrow 3d-4p transition, appeared at a slightly higher energy (8327.0 eV) than that of [Ni(cod)(2)] (8326.4 eV) with a shift of 0.6 eV (Figure 5b). This high-energy shift likely reflects a more electron-deficient Ni center in [Ni(cod)(1)] compared to [Ni(cod)(2)], due to the stronger electron-withdrawing nature of pentalene ligand 1. In addition, the subtracted pre-edge peak area followed the order of [Ni(cod)(1)] (0.37) $>$ [Ni(cod)(2)] (0.27) $>$ [Ni(cod)(dq)] (0.20) (Figure 5d, Table S3). Given the structural similarity of these complexes, this trend suggests that the Ni 3d electron occupancy decreases in the same order.

Further insights into the Ni electronic structure were obtained by Ni L_{2,3}-edge XAS, which probes the Ni 2p \rightarrow 3d transitions and thus directly reflects the Ni 3d electronic states. The L₃-edge peak maximum of [Ni(cod)(1)] appeared at 853.8 eV, which is 0.4 eV higher than that of [Ni(cod)(2)] (853.4 eV, Figure 5c). Moreover, the sum of the L₂- and L₃-edge integrated intensity of the main peaks was noticeably larger for [Ni(cod)(1)] (9.0) than for [Ni(cod)(2)] (7.8), indicating a lower Ni 3d electron occupancy in [Ni(cod)(1)].^{18,19} These trends align with the results from the pre-edge peak analysis of Ni K-edge XAS. Although these values are slightly higher than that of [Ni(cod)(dq)] (7.0), which is known as a stable Ni(0) complex, the differences remain modest, suggesting that the Ni centers in [Ni(cod)(1)] and [Ni(cod)(2)] adopt a d¹⁰-like electronic configuration. Accordingly, the contribution of the dianionic character in the pentalene ligand (i.e., Ni(II)-pentalene dianion complex), which would imply the acquisition of aromatic stabilization, appears unlikely. Meanwhile, [Ni(cod)(1)] and [Ni(cod)(dq)] exhibited distinct second peaks in the higher-energy region, with the integrated intensities of 5.2 and 4.8, respectively (Figure 5d, Table S3), whereas that of [Ni(cod)(2)] was substantially lower at 1.9. These higher-energy side bands have been attributed to metal-to-ligand charge transfer (MLCT) transitions, whose intensities are known to correlate with the degree of π -back donation.^{20,21} Accordingly, the pronounced second peaks for [Ni(cod)(1)] and [Ni(cod)(dq)] suggest substantial π -back donation from Ni to the ligand, in contrast to the reduced π -back donation in [Ni(cod)(2)].

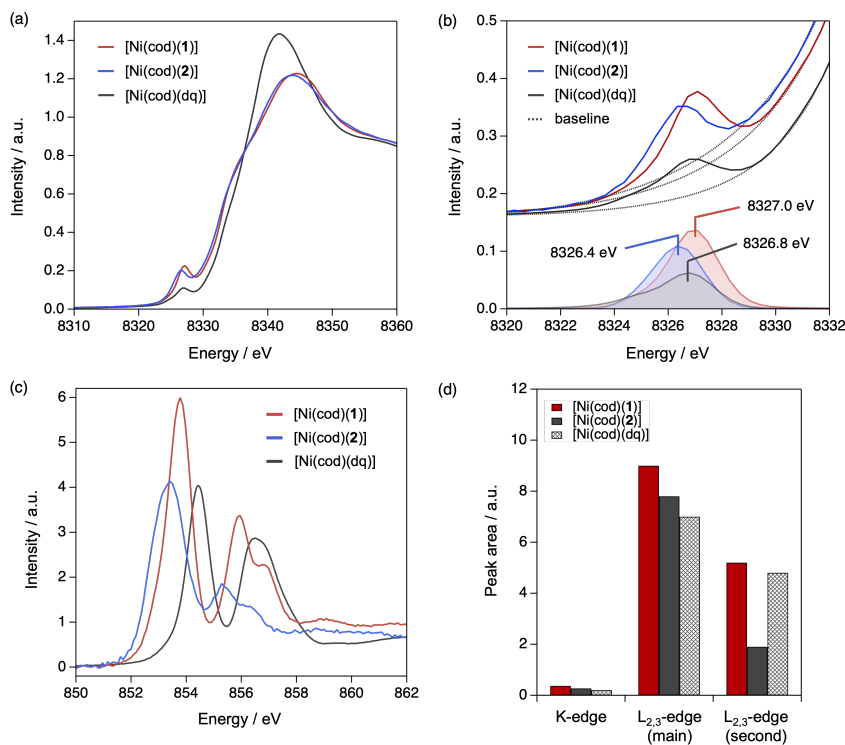


Figure 5. Experimental analyses for electronic structure and nickel–ligand interaction of Ni–pentalene complexes. (a) Ni K-edge XANES data. (b) Magnification of pre-edge region and subtracted spectra. (c) Ni L₃-edge XAS data. (d) Bar plots for Ni K-edge (pre-edge) and L_{2,3}-edge integrated peak intensity.

To quantitatively compare the strength of π -back donation, energy decomposition analyses (EDA) based on quantum chemical calculations were performed. Breakdowns of the interaction energies between the Ni(cod) fragment and a π ligand as illustrated in Figure 6a were estimated for [Ni(cod)(1)], [Ni(cod)(2)], [Ni(cod)(dq)], and Ni(cod)₂ using the absolutely localized molecular orbital (ALMO-EDA) method using ω B97X-D/def2-TZVP level.²² The total stabilization energy for [Ni(cod)(1)] was found to be $-95.5\text{ kcal mol}^{-1}$, which was significantly larger than that for [Ni(cod)(2)] of $-74.7\text{ kcal mol}^{-1}$ (Table S7). This trend is consistent with the relative stabilities of these Ni complexes observed experimentally. Whereas the contribution of dispersion and polarization interaction terms was small (ca. 10% each) and minimal variation among these four complexes, the electrostatic and charge-transfer (CT) interaction terms exhibit a major contribution to the interaction (Figure 6b). More specifically, the contribution of CT term, which represents the significance of orbital interaction including π -back donation, was markedly greater in [Ni(cod)(1)] (40.7%) than in [Ni(cod)(2)] (36.4%), and even more so compared to [Ni(cod)(dq)] (34.9%) and [Ni(cod)₂] (28.4%). This difference indicates that an exceptionally strong orbital interaction exists between Ni(cod) and pentalene **1** compared to other ligands. Further energy decomposition of the CT

component into forward charge transfer (CT_f , from the ligand to the Ni(cod) fragment) and backward charge transfer (CT_b , from the Ni(cod) fragment to the ligand) by variational forward–backward CT analysis (CTA-VFB) scheme²³ revealed that CT_b is the dominant contributor to the CT component in all four complexes (Figure 6c). The magnitude of the CT_b stabilization followed the order $[\text{Ni}(\text{cod})(\mathbf{1})] > [\text{Ni}(\text{cod})(\mathbf{2})] > [\text{Ni}(\text{cod})(\text{dq})] > \text{Ni}(\text{cod})_2$, with $[\text{Ni}(\text{cod})(\mathbf{1})]$ showing the most significant stabilization ($-98.2 \text{ kcal mol}^{-1}$), which was notably greater than that of $[\text{Ni}(\text{cod})(\mathbf{2})]$ ($-86.6 \text{ kcal mol}^{-1}$). Given that CT_b corresponds to the π -back donation from the Ni center to the ligand, these results quantitatively demonstrate that $[\text{Ni}(\text{cod})(\mathbf{1})]$ exhibits a more substantial π -back donation than $[\text{Ni}(\text{cod})(\mathbf{2})]$ or the other Ni(0) complexes, showing a good coincidence with the result from XAS analysis. Taken together with both experimental and computational data, these findings indicate that the strong π -back donation from Ni to the ligand governs the interaction between the pentalene framework and the Ni center. In other words, the low-lying LUMO of the pentalene ligand plays a more crucial role in stabilizing the complex rather than the effect of the antiaromaticity relief.

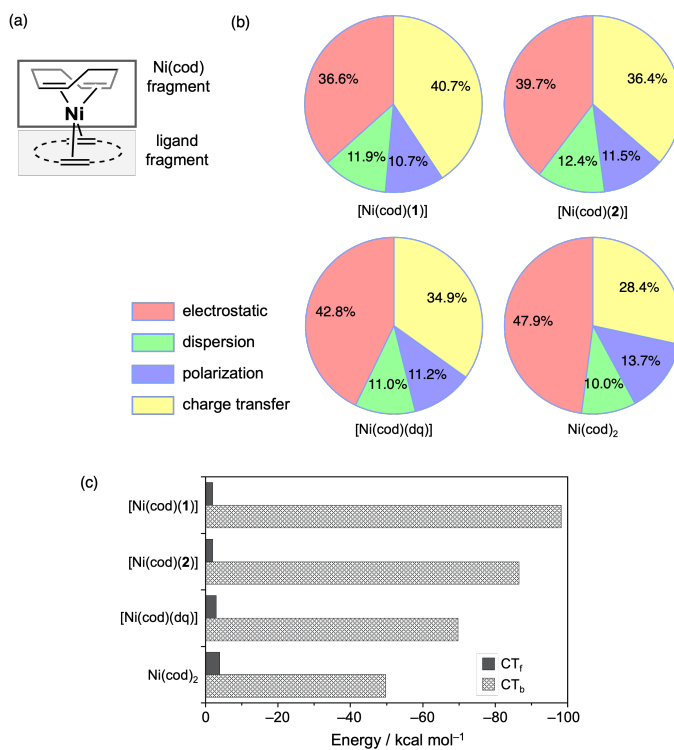


Figure 6. Energy decomposition analyses for Ni–ligand interaction of Ni–pentalene complexes. (a) Schematic representation of the decomposition analysis of the Ni complexes. (b) EDA results in 2D pie charts for the ratio of the contribution of interaction energies between the Ni(cod) fragment and a ligand based on the ALMO-EDA method. The results for $[\text{Ni}(\text{cod})(\text{dq})]$ and $\text{Ni}(\text{cod})_2$ are also shown for reference. (c) Breakdown of charge transfer (CT) interactions obtained via CTA-VFB analysis. CT_b and CT_f correspond

to backward (from the Ni(cod) fragment to a ligand) and forward components (from a ligand to the Ni(cod) fragment), respectively.

Fluxional Behavior of [Ni(cod)(1)] in Solution. Despite the strong coordination interaction between Ni and the benzothiophene-*S,S*-dioxide-fused pentalene **1** revealed above, [Ni(cod)(1)] was found to exhibit pronounced dynamic behavior in solution. As already characterized by single-crystal X-ray diffraction analysis, the Ni atom resides above one of the two five-membered rings of the pentalene unit in the solid state, coordinating in an η^4 -mode to the *s-cis*-butadiene substructure (Figure 2a). On the other hand, the ^1H NMR spectrum of a CD₂Cl₂ solution of [Ni(cod)(1)] recorded at 298 K revealed only four distinct resonance signals assignable to protons H^a–H^d on the benzene rings of benzothiophene moiety in the pentalene ligand, and three signals corresponding to protons H^e–H^g on the phenyl groups at the 1,4-positions of the pentalene (Figure 7). This spectral pattern indicates that the Ni center rapidly migrates between the two five-membered rings of the pentalene framework on the NMR timescale at this temperature, resulting in time-averaged signals. As the temperature is decreased from 298 K to 238 K, these resonance signals began to split, indicating the suppression of the migration process. More specifically, the signal at 7.87 ppm, assigned to either H^a or H^d, underwent coalescences at 278 K and resolves into two separate signals at lower temperatures. Similarly, the signal assigned to H^e at 8.25 ppm coalesces at 283 K and splits into two distinct resonances below this temperature. Considering that rotational dynamics of the phenyl rings may also influence the temperature dependence of the H^e signal, the activation barrier (ΔG^\ddagger) for the ring-to-ring migration of the Ni center was estimated based on the coalescence temperature of the H^a or H^d signals, yielding an ΔG^\ddagger of 13.6 kcal mol⁻¹.

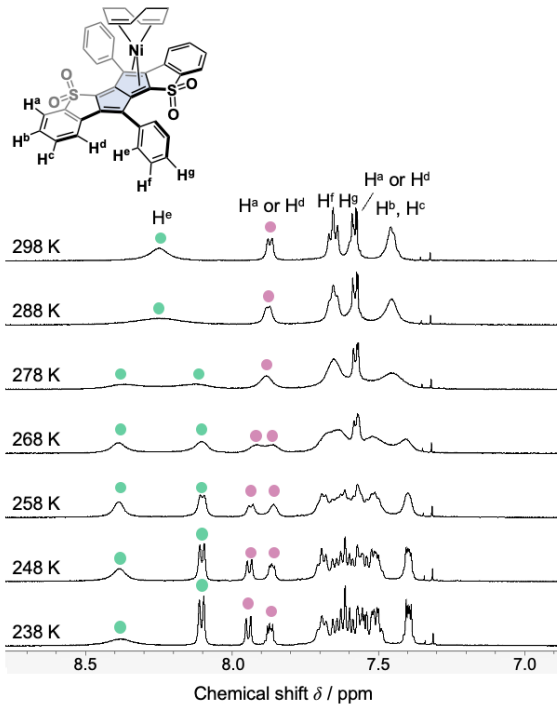


Figure 7. Variable-temperature ^1H NMR spectra of $[\text{Ni}(\text{cod})(\mathbf{1})]$ recorded from 298 to 238 K (500 MHz, in CD_2Cl_2). Selected signals are annotated to indicate their assignments.

To gain further insight into the structural dynamics associated with the fluxional behavior of the Ni center, we performed quantum chemical calculations, including geometry optimizations and intrinsic reaction coordinate (IRC) analyses of the putative intermediates and transition states at the $\omega\text{B97X-D/LanL2DZ}$ (for Ni) and 6-31G(d) (for C, H, O, S) level of theory. As a result, the interconversion involving the migration of Ni between the two fused five-membered rings of pentalene proceeds via a two-step mechanism (Figure 8a). In the first step, starting from an initial structure (**R**) where the Ni center coordinates in an η^4 -fashion to one of the five-membered rings, a haptotropic shift occurs along the periphery of the pentalene ligand, through a transition state **TS1** and leading to an intermediate (**Int**) in which the Ni center is bound to the other five-membered ring (Figure 8a,b). A detailed analysis of the C–C bond lengths within the pentalene framework revealed that this Ni migration is accompanied by a reorganization of the bond length alternation. For instance, the C–C bond annulated with the benzothiophene-*S,S*-dioxide units is single bond-like (1.48 Å) in **R** but double bond-like (1.39 Å) in **Int** (Figure 8c), indicating that the movement of the Ni center induces a bond shift across the pentalene scaffold. In the subsequent second step, **Int** proceeds via a transition state **TS2** to afford the final structure (**R'**), which is virtually equivalent to the initial state **R**. Interestingly, this step does not involve significant migration of the Ni center but rather a reorganization of the C–C double bonds within the pentalene ligand and a

rotation of the Ni(cod) fragment. The latter rotational motion is most likely to optimize orbital overlap between the Ni 3d orbitals and the π orbitals of the *s-cis* butadiene moiety, in response to the bond shift within the pentalene ligand.

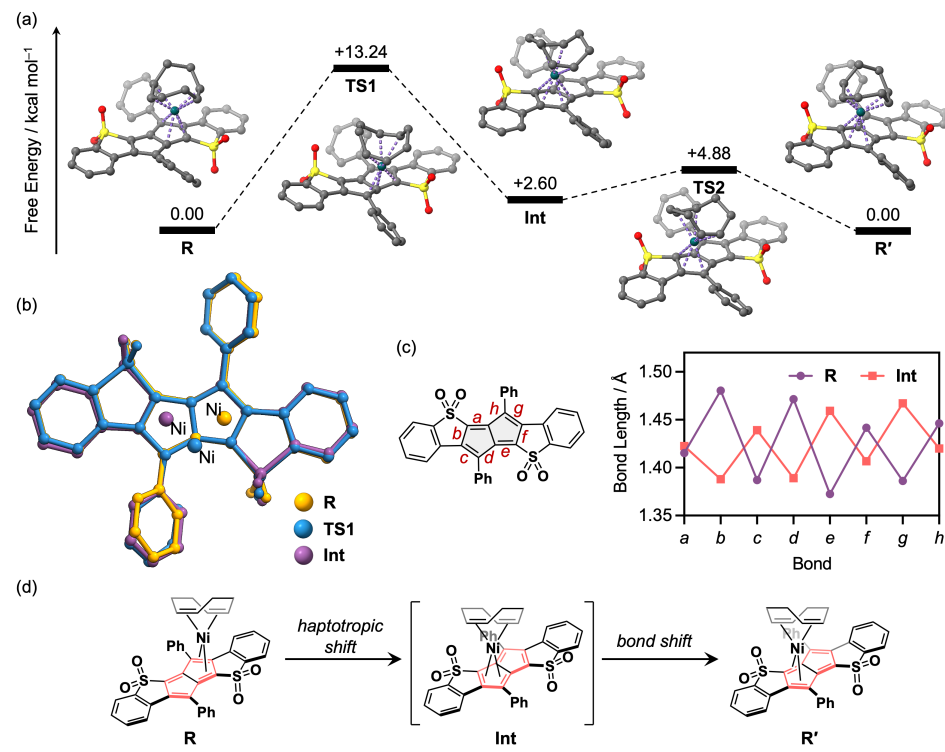


Figure 8. Mechanistic studies of the fluxional behavior of $[\text{Ni}(\text{cod})(\mathbf{1})]$ based on DFT calculations. (a) Calculated energy profile for the intramolecular migration of the Ni(cod) fragment between the two five-membered rings at $\omega\text{B97X-D}/\text{def2-TZVP}$, based on geometry optimizations and intrinsic reaction coordinate (IRC) analysis at the $\omega\text{B97X-D}/\text{LanL2DZ}$ (for Ni) and 6-31G(d) (for C, H, O, S) level of theory. **R** and **R'** denote the equivalent ground-state structures, **Int** represents an intermediate, and **TS1** and **TS2** are transition states. (b) Top-view representations of the Ni and the pentalene ligand extracted from the optimized geometries of **R** (orange), **TS1** (blue), and **Int** (purple). Hydrogen atoms and cod ligands are omitted for clarity. (c) Plot of selected C–C bond lengths in the pentalene framework in the optimized geometries of **R** (purple) and **Int** (red). (d) Plausible mechanism of the fluxional behavior of $[\text{Ni}(\text{cod})(\mathbf{1})]$.

The computed activation energies $\Delta G_{\text{calc}}^{\ddagger}$ for these two-step isomerization processes were 13.24 kcal mol⁻¹ and 2.28 kcal mol⁻¹, respectively, at $\omega\text{B97X-D}/\text{def2-TZVP}$ level of theory using optimized geometries, indicating that the initial Ni migration constitutes the rate-determining step. The value of $\Delta G_{\text{calc}}^{\ddagger}$ for the first step is in reasonable agreement with that estimated from variable-temperature NMR experiments (13.6 kcal mol⁻¹), and is sufficiently low to account for the observed fluxional behavior. Notably, this

activation barrier is significantly lower than those reported for haptotropic shifts in relevant η^4 -olefin complexes of other fourth-row transition metals, such as $[\text{Fe}(\text{CO})_3(\eta^4\text{-1,6-diaryl-1,3,5-hexatriene})]$ ($\Delta G^\ddagger = 33.0 \text{ kcal mol}^{-1}$)²⁴ and $[\text{Fe}(\text{CO})_3(\eta^4\text{-cycloheptatriene})]$ ($\Delta G^\ddagger = 22.3\text{--}23.9 \text{ kcal mol}^{-1}$).²⁵ These results highlight the exceptionally high fluxionality of the pentalene-Ni coordination framework. While the relationship between this fluxional behavior and the antiaromatic character of the pentalene ligand remains unclear, it represents a noteworthy feature of this system.

CONCLUSIONS

In summary, we have synthesized and characterized a Ni(0) complex $[\text{Ni}(\text{cod})(\mathbf{1})]$ featuring a benzothiophene-*S,S*-dioxide-fused pentalene as a ligand, and quantitatively evaluated its bonding interactions through comparison with its analogue $[\text{Ni}(\text{cod})(\mathbf{2})]$ bearing a more antiaromatic but less electron-accepting ligand. The results reveal that the enhanced stability of $[\text{Ni}(\text{cod})(\mathbf{1})]$ arises primarily from strong π -back donation enabled by the unusually low-lying LUMO of the ligand, rather than from the relief of its antiaromatic character. This result underscores that, in transition metal complexes of antiaromatic hydrocarbons, specific electronic factors such as low-lying LUMOs can provide a more direct explanation for bonding interactions than the broader concept of antiaromaticity. More broadly, these findings also serve as a reminder that antiaromaticity is not a directly measurable physical quantity, but rather a conceptual framework encompassing multiple correlated features, such as intrinsic instability,^{1,2} bond length alternation induced by pseudo-Jahn–Teller distortions,^{26,27} and paratropic ring currents.²⁸ Shifting the focus from this abstract label to underlying, quantifiable properties may help clarify which aspects of antiaromatic systems most directly influence their chemical behavior of interest, offering a path to a more predictive understanding of their coordination chemistry.

Another important finding of this study is the pronounced fluxional behavior of $[\text{Ni}(\text{cod})(\mathbf{1})]$ in solution, involving reversible migration of the Ni center between the two fused five-membered rings. This is particularly intriguing given the strong π -back donation that characterizes the Ni–pentalene interaction. DFT calculations suggest this dynamic process is accompanied by a reorganization of C=C bonds within the pentalene framework, indicating that the carbon skeleton actively participates in the structural rearrangement. While the relationship between this fluxionality and the antiaromatic nature of the ligand remains to be clarified, such behavior may reflect bond shifting in the carbon framework, which is one of the structural characteristics of antiaromatic systems. Further investigation into this aspect is underway.

ASSOCIATED CONTENT

Deposition Numbers 2451621 and 2451622 contain the supplementary crystallographic data for this paper. These data can be obtained free of charge via the joint Cambridge Crystallographic Data Centre (CCDC) and Fachinformationszentrum Karlsruhe [Access Structures service](#).

AUTHOR INFORMATION

Corresponding Author

Yuta Uetake – Department of Applied Chemistry, Graduate School of Engineering, The University of Osaka, Suita, Osaka 565-0871, Japan; Innovative Catalysis Science Division, Institute for Open and Transdisciplinary Research Initiatives (ICS-OTRI), The University of Osaka, Suita, Osaka 565-0871, Japan; orcid.org/0000-0002-4742-8085; Email: uetake@chem.eng.osaka-u.ac.jp

Aiko Fukazawa – Institute for Integrated Cell-Material Sciences (WPI-iCeMS), Institute for Advanced Study, Kyoto University, Yoshida, Sakyo-ku, Kyoto 606-8501, Japan; orcid.org/0000-0002-2903-105X; Email: afukazawa@icems.kyoto-u.ac.jp

Authors

Riina Kuwata – Department of Energy and Hydrocarbon Chemistry, Graduate School of Engineering, Kyoto University, Yoshida, Sakyo-ku, Kyoto 606-8501, Japan

Takefumi Imanishi – Department of Energy and Hydrocarbon Chemistry, Graduate School of Engineering, Kyoto University, Yoshida, Sakyo-ku, Kyoto 606-8501, Japan

Shota Hasegawa – Institute for Integrated Cell-Material Sciences (WPI-iCeMS), Institute for Advanced Study, Kyoto University, Yoshida, Sakyo-ku, Kyoto 606-8501, Japan; orcid.org/0000-0003-1502-0066

Zhe Wang – Institute for Integrated Cell-Material Sciences (WPI-iCeMS), Institute for Advanced Study, Kyoto University, Yoshida, Sakyo-ku, Kyoto 606-8501, Japan; orcid.org/0000-0002-9996-586X

Junichi Usuba – Institute for Integrated Cell-Material Sciences (WPI-iCeMS), Institute for Advanced Study, Kyoto University, Yoshida, Sakyo-ku, Kyoto 606-8501, Japan; orcid.org/0000-0002-7571-5276

Kosuke Yasui – Institute for Integrated Cell-Material Sciences (WPI-iCeMS), Institute for Advanced Study, Kyoto University, Yoshida, Sakyo-ku, Kyoto 606-8501, Japan; orcid.org/0000-0002-3906-8307

Present Addresses

Riina Kuwata – Department of Applied Chemistry, Graduate School of Engineering, The University of Osaka, Suita, Osaka 565-0871, Japan

Junichi Usuba – Center for Carbon-Free Society Creation, Institute of Future Society Creation, Nagoya University, Furo-cho, Chikusa-ku, Nagoya 464-8603, Japan

Kosuke Yasui – Department of Applied Chemistry, Graduate School of Engineering, The University of Osaka, Suita, Osaka 565-0871, Japan

Author Contributions

R.K. and T.I. contributed equally to this work.

Funding Sources

This work was partially supported by JSPS KAKENHI Grant Numbers 20H05864, 21H01916, and 24H00458 (to A.F.), 22K05095 and 24H01851 (to Y.U.), and 23K19271 (to S.H.).

Notes

The authors declare no competing financial interests.

ACKNOWLEDGMENT

The authors thank the iCeMS Analysis Center for providing access to the NMR spectrometer. The synchrotron single-crystal X-ray diffraction measurements and Ni K-edge XAS measurements were performed at the BL02B1 and the BL14B2 beamlines of SPring-8, respectively, with the approval of the Japan Synchrotron Radiation Research Institute (JASRI; project no. 2022A1705 for SCXRD and 2022B1890, 2023B2061 for XAS). Ni L_{2,3}-edge XAS measurements were performed at the BL19B beamline of KEK under the approval of the Photon Factory Program Advisory Committee (proposal numbers 2022P0 and 2024G031). The authors are also grateful to Ms. Akiko Fujihashi and Ms. Eriko Kusaka (Kyoto University) for their technical support for the mass spectrometry and NMR spectroscopy, respectively.

REFERENCES

- (1) (a) Watts, L.; Fitzpatrick, J. D.; Pettit, R. Cyclobutadiene. *J. Am. Chem. Soc.* **1965**, *87*, 3253–3254. (b) Breslow, R.; Brown, J.; Gajewski, J. J. Antiaromaticity of Cyclopropenyl Anions. *J. Am. Chem. Soc.* **1967**, *89*, 4383–4390. (c) Breslow, R. Small Antiaromatic Rings. *Angew. Chem. Int. Ed. Engl.* **1968**, *7*, 565–570. (d) Lin, C. Y.; Krantz, A. Matrix Preparation of Cyclobutadiene. *J. Chem. Soc., Chem. Commun.* **1972**, 1111–1112. (e) Deniz, A. A.; Peters, K. S.; Snyder, G. J. Experimental Determination of the Antiaromaticity of Cyclobutadiene. *Science* **1999**, *286*, 1119–1122.
- (2) (a) Mayo, P. D.; Bloch, R.; Marty, R. A. Flash Thermolysis. VI. 1-Methylpentalene. *J. Am. Chem. Soc.* **1971**, *93*, 3071–3072. (b) Hafner, K.; Dönges, R.; Goedecke, E.; Kaiser, R. Concerning Pentalene, 2-Methylpentalene, and 1,3-Dimethylpentalene. *Angew. Chem. Int. Ed. Engl.* **1973**, *12*, 337–339. (c) Dönges, R.; Hafner, K.; Lindner, H. J. Bildung Und Isomerisierung Des Dimeren Pentalens. *Tetrahedron Lett.* **1976**, *17*, 1345–1348. (d) Bally, T.; Chai, S.; Neuenschwander, M.; Zhu, Z. Pentalene: Formation, Electronic, and Vibrational Structure. *J. Am. Chem. Soc.* **1997**, *119*, 1869–1875.
- (3) Reviews on cyclobutadiene–metal complexes: Shvydkiy, N. V.; Perekalin, D. S. Cyclobutadiene Complexes of Platinum Metals. *Coord. Chem. Rev.* **2017**, *349*, 156–168.
- (4) (a) Criegee, R.; Schröder, G. Ein Derivat Des Cyclobutadiens. *Liebigs Ann Chem* **1959**, *623*, 1–8. (b) Amiet, R. G.; Reeves, P. C.; Pettit, R. Cyclobutadiene–Metal Carbonyl Complexes. *Chem. Commun. (London)* **1967**, 1208–1208.

- (5) Reviews on pentalene–metal complexes: (a) Cloke, F. G. N. Organometallic Pentalene Complexes. *Pure Appl. Chem.* **2001**, *73*, 233–238. (b) Cloke, F. G. N.; Green, J. C.; Kilpatrick, A. F. R.; O’Hare, D. Bonding in Pentalene Complexes and Their Recent Applications. *Coord. Chem. Rev.* **2017**, *344*, 238–262.
- (6) (a) Katz, T. J.; Acton, N. Bis(Pentalenylnickel). *J. Am. Chem. Soc.* **1972**, *94*, 3281–3283. (b) Katz, T. J.; Acton, N.; McGinnis, J. Sandwiches of Iron and Cobalt with Pentalene. *J. Am. Chem. Soc.* **1972**, *94*, 6205–6206.
- (7) Howard, J. A. K.; Knox, S. A. R.; Riera, V.; Stone, F. G. A.; Woodward, P. Pentalene Complexes from Cyclo-Octatetraenes: Crystal Structure of Ru₃(CO)₈(C₈H₆). *J. Chem. Soc., Chem. Commun.* **1974**, 452–453.
- (8) Butenschön, H. Pentalene as a Complex Ligand: New Developments in the Chemistry of Nonalternant, Highly Unsaturated Hydrocarbons. *Angew. Chem. Int. Ed. Engl.* **1997**, *36*, 1695–1697.
- (9) Cloke, F. G. N.; Hitchcock, P. B. A New Class of Actinide “Sandwich” Complexes: Synthesis and Molecular Structure of a Thorium Bis(H₈-Pentalene) Complex. *J. Am. Chem. Soc.* **1997**, *119*, 7899–7900.
- (10) Bendjaballah, S.; Kahlal, S.; Costuas, K.; Bévillon, E.; Saillard, J. The Versatility of Pentalene Coordination to Transition Metals: A Density Functional Theory Investigation. *Chem. Eur. J.* **2006**, *12*, 2048–2065.
- (11) (a) Dewar, M. J. S. A Review of the pi-Complex Theory. *Bull. Soc. Chim. Fr.* **1951**, *18*, C71–79. (b) Chatt, J.; Duncanson, L. A. 586. Olefin Co-Ordination Compounds. Part III. Infra-Red Spectra and Structure: Attempted Preparation of Acetylene Complexes. *J. Chem. Soc.* **1953**, 2939–2947.
- (12) Usuba, J.; Hayakawa, M.; Yamaguchi, S.; Fukazawa, A. Dithieno[*a,e*]Pentalenes: Highly Antiaromatic Yet Stable π-Electron Systems without Bulky Substituents. *Chem. –Eur. J.* **2021**, *27*, 1638–1647.
- (13) Our reaction condition in ref. 12 was originally modified based on the conditions in the following reports: (a) Kawase, T.; Konishi, A.; Hirao, Y.; Matsumoto, K.; Kurata, H.; Kubo, T. An Extremely Simple Dibenzopentalene Synthesis from 2-Bromo-1-ethynylbenzenes Using Nickel(0) Complexes: Construction of Its Derivatives with Various Functionalities. *Chem. –Eur. J.* **2009**, *15*, 2653–2661. (b) Levi, Z. U.; Tilley, T. Versatile Synthesis of Pentalene Derivatives via the Pd-Catalyzed Homocoupling of Haloenynes. *J. Am. Chem. Soc.* **2009**, *131*, 2796–2797.
- (14) The analyses of the electron occupancy of the Ni 3d orbitals were conducted by X-ray absorption spectroscopy (XAS) and the quantum chemical calculations (NPA analysis) also supported that the oxidation state of the Ni center in [Ni(cod)(1)] is close to Ni(0).

(15) (a) Nattmann, L.; Saeb, R.; Nöthling, N.; Cornella, J. An Air-Stable Binary Ni(0)–Olefin Catalyst. *Nat. Catal.* **2020**, *3*, 6–13. (b) Nattmann, L.; Cornella, J. Ni(*4-t*Bustb)₃: A Robust 16-Electron Ni(0) Olefin Complex for Catalysis. *Organometallics* **2020**, *39*, 3295–3300. (c) Kuziola, J.; Magre, M.; Nöthling, N.; Cornella, J. Synthesis and Structure of Mono-, Di-, and Trinuclear Fluorotriarylbismuthonium Cations. *Organometallics* **2022**, *41*, 1754–1762.

(16) (a) Tran, V. T.; Li, Z.; Apolinar, O.; Derosa, J.; Joannou, M. V.; Wisniewski, S. R.; Eastgate, M. D.; Engle, K. M. Ni(COD)(DQ): An Air-Stable 18-Electron Nickel(0)–Olefin Precatalyst. *Angew. Chem. Int. Ed.* **2020**, *59*, 7409–7413. (b) Tran, V. T.; Kim, N.; Rubel, C. Z.; Wu, X.; Kang, T.; Jankins, T. C.; Li, Z.; Joannou, M. V.; Ayers, S.; Gembicky, M.; Bailey, J.; Sturgell, E. J.; Sanchez, B. B.; Chen, J. S.; Lin, S.; Eastgate, M. D.; Wisniewski, S. R.; Engle, K. M. Structurally Diverse Bench-Stable Nickel(0) Pre-Catalysts: A Practical Toolkit for In Situ Ligation Protocols. *Angew. Chem. Int. Ed.* **2023**, *62*, e202211794. (c) Rubel, C. Z.; He, W.-J.; Wisniewski, S. R.; Engle, K. M. Benchtop Nickel Catalysis Invigorated by Electron-Deficient Diene Ligands. *Acc. Chem. Res.* **2024**, *57*, 312–326.

(17) Geometry optimizations revealed that the pentalene cores in both **1** and **2** exhibit distinct bond alternation patterns; notably, the distribution of shorter and longer bonds is inverted between these compounds. Specifically, in **1**, the C–C bonds fused to the benzothiophene rings are single-bond-like, consistent with the structural trends observed for the pentalene ligand in the X-ray crystal structure of [Ni(cod)(**1**)], whereas, in **2**, the analogous fused C–C bonds are double-bond-like. This reversal in bond-length distribution leads to differences in the spatial distribution of the Kohn-Sham HOMOs and LUMOs, as illustrated in Figure 3b. See Supporting Information for further details. This difference is deliberately reflected in the structural representations of **1** and **2**, as well as their corresponding Ni complexes, throughout this paper.

(18) (a) Dimucci, I. M.; Lukens, J. T.; Chatterjee, S.; Carsch, K. M.; Titus, C. J.; Lee, S. J.; Nordlund, D.; Betley, T. A.; MacMillan, S. N.; Lancaster, K. M. The Myth of d₈ Copper(III). *J. Am. Chem. Soc.* **2019**, *141*, 18508–18520. (b) DiMucci, I. M.; Titus, C. J.; Nordlund, D.; Bour, J. R.; Chong, E.; Grigas, D. P.; Hu, C. H.; Kosobokov, M. D.; Martin, C. D.; Mirica, L. M.; Nebra, N.; Vicic, D. A.; Yorks, L. L.; Yruegas, S.; MacMillan, S. N.; Shearer, J.; Lancaster, K. M. Scrutinizing Formally Ni^{IV} centers through the lenses of core spectroscopy, molecular orbital theory, and valence bond theory. *Chem. Sci.* **2023**, *14*, 6915–6929.

(19) Mondori, Y.; Yamauchi, Y.; Kawakita, T.; Ogoshi, S.; Uetake, Y.; Takeichi, Y.; Sakurai, H.; Hoshimoto, Y. Monodentate σ-Accepting Boron-Based Ligands Bearing Square-Planar Ni(0) Centers. *J. Am. Chem. Soc.* **2025**, *147*, 8326–8335.

(20) Kosugi and coworkers demonstrated that these second bands in higher energy region originate from metal-to-ligand charge transfer (MLCT) transitions by polarized XAS and theoretical calculations. For

detail, see: Hatsui, T.; Kosugi, N. Metal-to-ligand charge transfer in polarized metal L-edge X-ray absorption of Ni and Cu Complexes. *J. Electron Spectrosc. Relat. Phenom.* **2004**, *136*, 67–75.

(21) Lancaster *et al.* demonstrated that the second peaks in Cu L_{2,3}-edge XAS exhibit significant ligand contributions, as confirmed by Cu K-edge XAS and resonant inelastic X-ray scattering (RIXS) analyses. For details, see ref. 18a.

(22) Horn, P. R.; Mao, Y.; Head-Gordon, M. Probing non-covalent interactions with a second generation energy decomposition analysis using absolutely localized molecular orbitals. *Phys. Chem. Chem. Phys.* **2016**, *18*, 23067–23079.

(23) Loipersberger, M.; Mao, Y.; Head-Gordon, M. Variational Forward–Backward Charge Transfer Analysis Based on Absolutely Localized Molecular Orbitals: Energetics and Molecular Properties. *J. Chem. Theory. Comput.* **2020**, *16*, 1073–1089.

(24) Whitlock, H. W.; Reich, C.; Woessner, W. D. Synthesis and Interconversion of Some Shift Isomeric Polyene-Tetrahaptoiron Tricarbonyl Complexes. *J. Am. Chem. Soc.* **1971**, *93*, 2483–2492.

(25) Karel, K. J.; Albright, T. A.; Brookhart, M. Fluxionality in (Cycloheptatriene)Iron Tricarbonyl Complexes. *Organometallics* **1982**, *1*, 419–430.

(26) Bersuker, I. B. Pseudo-Jahn–Teller Effect—A Two-State Paradigm in Formation, Deformation, and Transformation of Molecular Systems and Solids. *Chem. Rev.* **2013**, *113*, 1351–1390.

(27) Selected papers regarding the Pseudo-Jahn–Teller effect of antiaromatic hydrocarbons: (a) Kollmar, H.; Staemmler, V. A Theoretical Study of the Structure of Cyclobutadiene. *J. Am. Chem. Soc.* **1977**, *99*, 3583–3587. (b) Masamune, S.; Souto-Bachiller, F. A.; Machiguchi, T.; Bertie, J. E. Cyclobutadiene Is Not Square. *J. Am. Chem. Soc.* **1978**, *100*, 4889–4891. (c) Toyota, A.; Kataoka, M.; Koseki, S. Energy Component Analysis of the Pseudo Jahn-Teller Effect in Pentalene and Heptalene. *Chem. Lett.* **1992**, *221*, 791–794. (d) Toyota, A.; Koseki, S. Energy Component Analysis of the Pseudo-Jahn–Teller Effect in the Bicyclic Nonalternant Hydrocarbons: The Pentalenoid and Heptalenoid Systems. *J. Phys. Chem.* **1996**, *100*, 2100–2106. (e) Koseki, S.; Toyota, A. Energy Component Analysis of the Pseudo-Jahn–Teller Effect in the Ground and Electronically Excited States of the Cyclic Conjugated Hydrocarbons: Cyclobutadiene, Benzene, and Cyclooctatetraene. *J. Phys. Chem. A* **1997**, *101*, 5712–5718. (f) Shiota, Y.; Kondo, M.; Yoshizawa, K. Role of Molecular Distortions in the Spin–Orbit Coupling between the Singlet and Triplet States of the 4π Electron Systems C₄H₄, C₅H₅⁺, and C₃H₃[−]. *J. Chem. Phys.* **2001**, *115*, 9243–9254. (g) Pierrefixe, S. C. A. H.; Bickelhaupt, F. M. Aromaticity and Antiaromaticity in 4-, 6-, 8-, and 10-Membered Conjugated Hydrocarbon Rings. *J. Phys. Chem. A* **2008**, *112*, 12816–12822.

(28) (a) Wolovsky, R.; Sondheimer, F. Unsaturated Macroyclic Compounds. XXXVI. The Synthesis of Two Isomers of Bisdehydro[12]Annulene and Biphenylene from 1,5-Hexadiyne . *J. Am. Chem. Soc.* **1965**, *87*, 5720–5727. (b) Untch, K. G.; Wysocki, D. C. 5-Bromo-1,9-Bisdehydro[12]Annulene. Verification of an Induced Paramagnetic Ring Current in a $4n\pi$ -Electron System. *J. Am. Chem. Soc.* **1967**, *89*, 6386–6387. (c) Haddon, R. C. The Application of the Biot-Savart Law to the Ring Current Analysis of Proton Chemical Shifts—I A Comprehensive Investigation of the Annulenes. *Tetrahedron* **1972**, *28*, 3613–3633
